Indian J Pure Appl Math (2026) 57:808–825
https://doi.org/10.1007/s13226-024-00609-0

ORIGINAL RESEARCH

Modeling of fluid flow along a small heated irregularity on the plate surface in the framework of double-deck boundary layer structure

Roman K. Gaydukov

Received: 15 January 2023 / Accepted: 21 May 2024 / Published online: 31 May 2024

Abstract The paper is deals with the heat transfer in the laminar flow of a viscous incompressible fluid along a plate with a small heated localized irregularity. It is well known that double- and triple-deck structures of the boundary layer arise in such flow problems. These structures make it possible, among other things, to describe the phenomenon of separation of the boundary layer behind irregularities. In this paper, we study the heat transfer in the double-deck structure of the boundary layer. The asymptotic solution with double-deck structure is constructed for the problem under consideration for large Reynolds numbers. The results of numerical simulation of heat transfer in the region near the streamlined surface are presented. In particular, the effect of the presence of a separation zone (region with vortex) on heat transfer was studied, as well as the magnitude of the heat flux from the streamlined surface. The obtained results can be used in the design of cooling systems for microsized devices.

Keywords Double-deck structure · Heat transfer · Asymptotics · Numerical modeling

1 Introduction

In this paper, we investigate the temperature distribution in the problem of a heat-conducting incompressible viscous fluid laminar flow along a small heated localized irregularity on the plate surface for sufficiently large Reynolds numbers, but such that the flow is still laminar. To study the problems of fluid flow along surfaces with small irregularities, the models with multi-deck (double- and triple-deck) boundary layer structures are widely used, depending on the geometric scales of irregularities. The triple-deck structure of the boundary layer was discovered at the end of the 1960s independently by K. Stewartson, P. G. Williams [1] and V. Ya. Neiland [2], and it was first applied to the problem of flow along small hump-type irregularities by F. T. Smith [3]. The double-deck structure was discovered later independently by J. Mauss [4] (only the existence of this structure was shown) and V. G. Danilov [5] (equations describing this structure were obtained). These models have been actively studied since their discovery and have been applied to describe flows in various flow problems with various geometries.

In the framework of multi-deck models, the system of Navier–Stokes and continuity equations is reduced by various asymptotic methods to a set of simpler systems of equations describing flows in boundary layers (or "decks" in the terminology of this theory), which allow a simple and efficient numerical solution in contrast to another approach to such problems, namely, the direct numerical simulation (DNS) of the Navier–Stokes system of equations. The fact is that the presence of small irregularities on the streamlined surface generates several different spatial scales, which makes it rather difficult to use the DNS method due to its high cost of

Communicated by NM Bujurke.

R. K. Gaydukov (✉)
HSE University, 20 Myasnitskaya Ulitsa, Moscow 101000, Russia
E-mail: roma1990@gmail.com

computations, because it requires the use of high-performance computing clusters. But the resulting equations in the framework of multi-deck structures are good and can be efficiently solved numerically by using common personal computers. Note that these two approaches were compared in [6], where it was concluded that the multi-deck models adequately allow modeling these flow problems and can be used in real applications.

The heat transfer in the triple-deck model has recently been actively studied. In the series of works by I. I. Lipatov and M. V. Koroteev [7–10], the problem of a gas flow along a plate with flat local heated zones was studied. Namely, a supersonic flow with small temperature perturbations due to local heating zones was studied in [10], and, in particular, the effect of the length of the heating zone on the pressure distribution near the streamlined surface was studied. In [8,9], a similar problem was studied in the subsonic case, and it was shown that the flow disturbances decay exponentially both upstream and downstream in this case in contrast to the supersonic case in which they decay exponentially upstream. In the papers of A. F. Aljohani and J. S. B. Gajjar [11,12], the problem of a gas flow along heated hump-like irregularities on the plate surface for subsonic and transonic flows was studied for the triple-deck model. In particular, these papers show that non-planar heating elements cause larger pressure changes than flat elements.

However, despite the extensive study of heat transfer for the triple-deck model, similar problems have not been studied for the case of double-deck structure, and this is the main goal of this paper. Note that for the problem under consideration, an asymptotic solution with double-deck structure without taking into account the heating of the streamlined surface was previously constructed in [13–15].

The paper is organized as follows. Section 2 contains the mathematical formulation of the problem. In Section 3, an asymptotic solution of the problem under consideration is constructed. Section 4 presents the results of numerical simulation of the heat transfer near a streamlined surface.

2 Mathematical statement of the problem

We consider the problem of an incompressible heat-conducting viscous fluid flow along a semi-infinite plate with a small localized heated irregularity of arbitrary shape on its surface without gravity taken into account. Let the irregularity be localized at a distance $\hat{x}_0 > 0$ from the front edge of the plate fixed at the origin and co-directed with the $\hat{x}$ axis, see Fig. 1, and let the upstream flow be a parallel uniform flow with velocity $\hat{\mathbf{U}}_\infty = (\hat{u}_\infty, 0)$, constant density $\hat{\rho}_\infty$, pressure $\hat{p}_\infty$, and temperature $\hat{T}_\infty$. Looking ahead, note that we will consider the heating of only the irregularity itself, assuming that the plate temperature outside it is constant and equal to $\overline{T}$.

Let us introduce dimensionless coordinates $(x, y) = (\hat{x}, \hat{y})/\hat{x}_0$, dimensionless time $t = \hat{t}/\hat{t}_0$, dimensionless velocity $\mathbf{U} = \hat{\mathbf{U}}/\hat{u}_\infty$, dimensionless pressure $p = \hat{p}/(\hat{\rho}_\infty \hat{u}_\infty^2)$, and dimensionless temperature $T = \alpha(\hat{T} - \hat{T}_\infty)/(\hat{T}_w - \hat{T}_\infty) + 1$, where $\hat{t}_0$ is the characteristic time, $\hat{x}_0$ is the characteristic length, $\hat{u}_\infty$ is the characteristic speed, $\hat{T}_\infty$ is the characteristic temperature, $\hat{T}_w$ is the maximum temperature of the plate, α is the dimensionless scale coefficient, and the variables with "hat" are dimensional. For simulation (see Section 4) we put $\hat{T}_\infty = 300\,\mathrm{K}$, $\hat{T}_w = 360\,\mathrm{K}$, $\alpha = 9$, and $T_w = 10$ corresponds to $\hat{T}_w$. Note that in the dimensionless variables introduced above, the upstream plane-parallel flow will have velocity $\mathbf{U}_\infty = (1, 0)$, pressure p_∞, and temperature $T_\infty = 1$, and the irregularity will be localized at the point $x = 1$. We assume that the Reynolds number $\mathrm{Re} = \hat{u}_\infty \hat{x}_0 \hat{\rho}_\infty/\hat{\mu}$ is large enough but such that the boundary layer is laminar and the Prandtl number $\mathrm{Pr} = \hat{c}_p \hat{\mu}/\hat{\kappa}$ and the Eckert number $\mathrm{Ec} = \hat{u}_\infty^2 \alpha/(\hat{c}_p(\hat{T}_w - \hat{T}_\infty))$ are of order $O(1)$, where $\hat{\mu}$ is the dynamic viscosity of the fluid, $\hat{c}_p$ is the specific heat capacity of the medium at constant pressure, and $\hat{\kappa}$ is the thermal conductivity coefficient.

We consider the plate surface as

$$y_s = \varepsilon^{4/3} h\big((x-1)/\varepsilon\big), \tag{1}$$

where $\varepsilon = \mathrm{Re}^{-1/2}$ is a small parameter, $x = 1$ is the point at which the irregularity is localized, $h(\xi)$ is a smooth function describing the shape of the irregularity such that $\lim\limits_{\xi\to\pm\infty} h(\xi) = 0$, $\xi = (x-1)/\varepsilon$. Note that the chosen geometric scales (amplitude and width of the irregularity given by powers of a small parameter ε) generate the double-deck structure of the boundary layer, see [5,13–15] and Fig. 1.

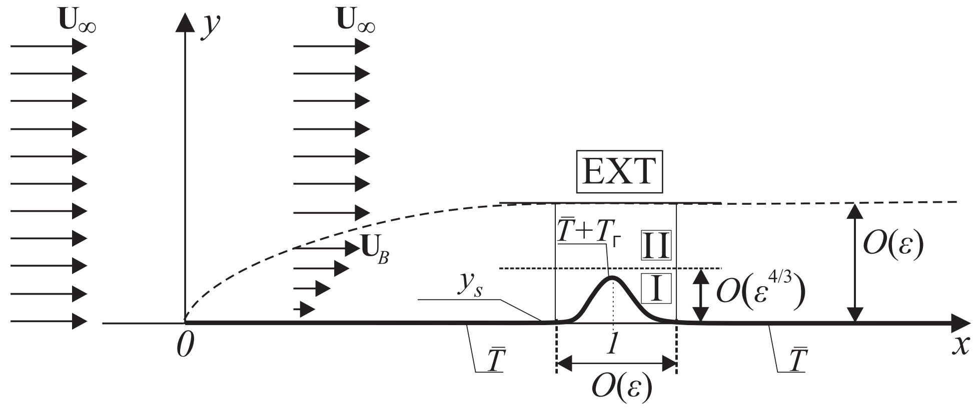

Fig. 1 A plate with small irregularity (dimensionless variables) and the double-deck boundary layer structure. Notation: I is the lower deck (the thin boundary layer); II is the middle deck (classical Prandtl boundary layer); EXT is the region with external (potential) flow, $\mathbf{U}_B$ is the flow with Blasius velocity profile (13)

The problem is described by the system of Navier–Stokes, continuity, and heat (with advection) equations

$$\varepsilon^{-2/3}\frac{\partial \mathbf{U}}{\partial t} + \langle \mathbf{u}, \nabla\rangle\mathbf{U} = -\nabla p + \varepsilon^2\Delta\mathbf{U}, \tag{2}$$

$$\langle \nabla, \mathbf{U}\rangle = 0, \tag{3}$$

$$\varepsilon^{-2/3}\frac{\partial T}{\partial t} + \langle \mathbf{U}, \nabla T\rangle = \frac{\varepsilon^2}{\mathrm{Pr}}\Delta T + \varepsilon^2\,\mathrm{Ec}\,\Phi, \tag{4}$$

where $\mathbf{U} = (u(t,x,y), v(t,x,y))$ is the $2D$ velocity vector, $p = p(t,x,y)$ is the pressure, $T = T(t,x,y)$ is the temperature, and the dissipation function Φ has the form

$$\Phi = 2\left(\frac{\partial u}{\partial x}\right)^2 + 2\left(\frac{\partial v}{\partial y}\right)^2 + \left(\frac{\partial u}{\partial y} + \frac{\partial v}{\partial x}\right)^2. \tag{5}$$

Note that the presence of the coefficient $\varepsilon^{-2/3}$ at the time derivative is due to the choice of the time scale. Namely, there also arises a hierarchy of times in the layers of non-stationary multi-deck structures in addition to multiple spatial scales, see [16–18], and considering the flow in the lower deck (the layer near the streamlined surface, see the domain I in Fig. 1) at finite times (i.e., the choice of an appropriate time scale, see (24) below) leads to the appearance of this coefficient.

System (2)–(5) is supplemented with the no-slip boundary condition on the streamlined surface, a given temperature on the surface, and some conditions for matching with the upstream flow:

$$\begin{gathered}\mathbf{U}\big|_{y=y_s} = 0,\ T\big|_{y=y_s} = \overline{T} + T_\Gamma(\xi),\\ \mathbf{U}\big|_{\substack{y\to\infty\\x>0}} = \mathbf{U}\big|_{x\to-\infty} = (1,0),\ T\big|_{\substack{y\to\infty\\x>0}} = T\big|_{x\to-\infty} = 1,\end{gathered} \tag{6}$$

where T_Γ is a given function describing the heating in the region of roughness such that $T_\Gamma\big|_{\xi\to\pm\infty} = 0$ and the temperature of the plate is constant $\overline{T} = \mathrm{const}$. System (2)–(5) is also supplemented with some smooth initial data, see for more details below.

3 Asymptotic solution with double-deck structure

Let us construct a formal asymptotic solution of problem (1)–(6). The algorithm for constructing the asymptotic solution with double-deck boundary layer structure is based on a combination of the boundary layer expansion method (using ideas from the paper by M. I. Vishik and L. A. Lyusternik [19]) and the method for constructing localized solutions (the presence of a small irregularity on the streamlined surface (i.e., a small perturbation of the boundary) does not affect the flow at far distances in front of it and behind it).

Now we introduce a new vertical variable $z = y - y_s$ such that the lower boundary (streamlined surface) becomes flat $z_s = 0$ in the variables (x, z), and we introduce boundary-layer variables (characteristic scales in the decks): the variables (ξ, θ) in the lower deck (see region I in Fig. 1) , and the variables (ξ, τ) in the middle deck (see region II in Fig. 1), where $\xi = (x-1)/\varepsilon$, $\theta = z/\varepsilon^{4/3}$, and $\tau = z/\varepsilon$.

We will look for a solution to problem (2)–(6) in the form

$$u(t,x,z) = 1 + u_0^{\mathrm{II}}(t,x,\tau) + \sum_{i\geq 1} \varepsilon^{i/3}\big(u_i^{\mathrm{ext}}(t,x,\xi,z) + u_i^{\mathrm{II}}(t,x,\xi,\tau) + u_i^{\mathrm{I}}(t,\xi,\theta)\big), \tag{7}$$

$$v(t,x,z) = \sum_{i\geq 2} \varepsilon^{i/3}\big(v_i^{\mathrm{ext}}(t,x,\xi,z) + v_i^{\mathrm{II}}(t,x,\xi,\tau) + v_i^{\mathrm{I}}(t,\xi,\theta)\big), \tag{8}$$

$$p(t,x,z) = p_\infty + \sum_{i\geq 1} \varepsilon^{i/3}\big(p_i^{\mathrm{ext}}(t,x,\xi,z) + p_i^{\mathrm{II}}(t,x,\xi,\tau) + p_i^{\mathrm{I}}(t,\xi,\theta)\big), \tag{9}$$

$$T(t,x,z) = 1 + T_0^{\mathrm{II}}(t,x,\tau) + T_0^{\mathrm{I}}(t,\xi,\theta) + \sum_{i\geq 1} \varepsilon^{i/3}\big(T_i^{\mathrm{ext}}(t,x,\xi,z) + T_i^{\mathrm{II}}(t,x,\xi,\tau) + T_i^{\mathrm{I}}(t,\xi,\theta)\big), \tag{10}$$

where the superscript ext denotes corrections to the external flow, and the Roman superscript on the functions denotes the deck of the double-deck structure (see Fig. 1) in which they are defined. Namely, the functions with superscripts I and II are boundary-layer functions, i.e., they decrease by the law θ^{-N} as $\theta \to \infty$ or τ^{-N} as $\tau \to \infty$, respectively, where $N \in \mathbb{N}$ is a sufficiently large number.

The algorithm for constructing the asymptotic solution with double-deck structure is as follows. First, we need to substitute expansions (7)–(10) into system (2)–(5) and collect the coefficients at the same powers of a small parameter ε. As a result, a certain family $\mathcal{E}$ of equations will be obtained.

Now let the boundary layer variables $\theta \to \infty$ and $\tau \to \infty$ in the family $\mathcal{E}$ of equations. As a result, we obtain systems of equations for corrections to the external flow (region EXT in Fig. 1). We denote them by $\mathcal{E}^{\mathrm{ext}}$.

Now let the thin boundary-layer variable $\theta \to \infty$ in $\mathcal{E}$. We take the results from $\mathcal{E}^{\mathrm{ext}}$ into account. At the current stage, we will use the asymptotic formula[1] for the products of functions from different regions $a^{\mathrm{ext}}(\circ, z)b^{\mathrm{II}}(\circ,\tau) = a^{\mathrm{ext}}(\circ, \varepsilon\tau)b^{\mathrm{II}}(\circ,\tau) = a^{\mathrm{ext}}\big|_{z=0}b^{\mathrm{II}} + \varepsilon\tau\frac{\partial a^{\mathrm{ext}}}{\partial z}\big|_{z=0}b^{\mathrm{II}} + O(\varepsilon^2)$ as $\varepsilon \to 0$. The result is the system of equations describing the flow in the middle deck (region II in Fig. 1). We denote them by $\mathcal{E}^{\mathrm{II}}$.

Next, we need to take into account the results from $\mathcal{E}^{\mathrm{ext}}$ and $\mathcal{E}^{\mathrm{II}}$ in the family of equations $\mathcal{E}$ obtained at the initial stage and use asymptotic formulas for products of functions from different regions $a^{\mathrm{ext}}(\circ, z)c^{\mathrm{I}}(\circ,\theta) = a^{\mathrm{ext}}(\circ, \varepsilon^{4/3}\theta)c^{\mathrm{I}}(\circ,\theta) = a^{\mathrm{ext}}\big|_{z=0}c^{\mathrm{I}} + \varepsilon^{4/3}\theta\frac{\partial a^{\mathrm{ext}}}{\partial z}\big|_{z=0}c^{\mathrm{I}} + O(\varepsilon^{8/3})$, $b^{\mathrm{II}}(\circ,\tau)c^{\mathrm{I}}(\circ,\theta) = b^{\mathrm{II}}(\circ,\varepsilon^{1/3}\theta)c^{\mathrm{I}}(\circ,\theta) = b^{\mathrm{II}}\big|_{\tau=0}c^{\mathrm{I}} + \varepsilon^{1/3}\theta\frac{\partial b^{\mathrm{II}}}{\partial \tau}\big|_{\tau=0}c^{\mathrm{I}} + O(\varepsilon^{2/3})$ as $\varepsilon \to 0$. The result is the system of equations describing the flow in the lower deck (region I in Fig. 1). We denote them by $\mathcal{E}^{\mathrm{I}}$.

To complete the solution construction, we need to obtain boundary conditions. This can be done by substituting expansions (7)–(10) in boundary conditions (6) taking into account the results obtained from $\mathcal{E}^{\mathrm{ext}}$, $\mathcal{E}^{\mathrm{II}}$, and $\mathcal{E}^{\mathrm{I}}$.

Note that at each stage of the algorithm described above, it is also necessary to use the method for constructing localized solutions. Namely, we suppose that the presence of a small irregularity does not affect the flow at far distances in front of it and behind it, i.e., the flow outside a neighborhood of the irregularity is a solution u_{np}, v_{np}, p_{np}, T_{np} to the unperturbed problem (i.e., for $h \equiv 0$):

$$(u, v, p, T)\big|_{\xi\to\pm\infty} \to (u_{np}, v_{np}, p_{np}, T_{np}). \tag{11}$$

In the stationary case, the solution of the unperturbed problem is well known [20,21] and has the form:

$$u_{nps} = 1 + u_{0,nps}^{\mathrm{II}}(x,\tau) + O(\varepsilon),\ v_{nps} = \varepsilon\big(v_{3,nps}^{\mathrm{II}}(x,\tau) + v_{3,nps}^{\mathrm{ext}}(x,z)\big) + O(\varepsilon^2),$$
$$p_{nps} = p_\infty + O(\varepsilon),\ T_{nps} = 1 + T_{0,nps}^{\mathrm{II}}(x,\tau) + O(\varepsilon), \tag{12}$$

where $u_{0,nps}^{\mathrm{II}} = f'(\tau/\sqrt{x}) - 1$, $v_{3,nps}^{\mathrm{II}} + v_{3,nps}^{\mathrm{ext}}\big|_{z=0} = \frac{1}{2\sqrt{x}}\big(f'(\tau/\sqrt{x})\frac{\tau}{\sqrt{x}} - f(\tau/\sqrt{x})\big)$, $v_{3,nps}^{\mathrm{ext}}$ is a solution of the Dirichlet problem for the Laplace equation[2], $T_{0,nps}^{\mathrm{II}} = g(\tau/\sqrt{x})(\overline{T}-1) + q(\tau/\sqrt{x})$, $f(\gamma)$ is the Blasius

[1] The notation $\circ$ means any other variables on which the functions depend

[2] The explicit form of this function is not of interest in the framework of this work, see Theorem 1

function which is determined from the boundary value problem for the ODE:

$$2f'''(\gamma) = -f(\gamma)f''(\gamma), \quad f(0) = f'(0) = 0, \quad f'(\infty) = 1, \tag{13}$$

and the functions $g(\gamma)$ and $q(\gamma)$ are solutions of the following boundary value problems for the ODE:

$$g''(\gamma)/Pr + f(\gamma)g'(\gamma)/2 = 0, \quad g(0) = 1, \quad g(\infty) = 0, \tag{14}$$
$$q''(\gamma)/Pr + f(\gamma)q'(\gamma)/2 + \mathrm{Ec}(f''(\gamma))^2 = 0, \quad q(0) = 0, \quad q(\infty) = 0. \tag{15}$$

It follows from the previously noted specific feature of the chosen time scale (see (2)–(5)) in the problem studied in this paper (see [15,17]) that all equations describing the main flow are considered at small times. For example, the system of Prandtl boundary layer equations has the form

$$\varepsilon^{-2/3}\frac{\partial u^\dagger}{\partial t} + u^\dagger\frac{\partial u^\dagger}{\partial x} + v^\dagger\frac{\partial u^\dagger}{\partial \tau} = \frac{\partial^2 u^\dagger}{\partial \tau^2}, \quad \frac{\partial u^\dagger}{\partial x} + \frac{\partial v^\dagger}{\partial \tau} = 0,$$

where $u^\dagger = 1 + u^{\mathrm{II}}_{0,np}$, $v^\dagger = v^{\mathrm{II}}_{3,np} + v^{\mathrm{ext}}_{3,np}\big|_{z=0}$. Obviously, if we consider the Cauchy problem for this equation with the stationary flow as the initial data, then the solution at small times $\varepsilon^{2/3}t$ will have the form

$$u^\dagger = f'(\tau/\sqrt{x}) + O(\varepsilon^{2/3}).$$

So we take the following initial data for the problem (1)–(6):

$$u\big|_{t=0} = f'(\tau/\sqrt{x}) + \varepsilon^{1/3}U^*(\xi, \theta 0) + O(\varepsilon^{2/3}), \tag{16}$$
$$v\big|_{t=0} = \varepsilon^{2/3}V^{\mathrm{II}}(\xi, \tau) + O(\varepsilon), \tag{17}$$
$$T\big|_{t=0} = 1 + g(\tau/\sqrt{x})(\overline{T} - 1) + q(\tau/\sqrt{x}) + T^*(\xi, \theta) + O(\varepsilon^{1/3}), \tag{18}$$

where the main terms of these expansions are the stationary solution of the unperturbed problem u_{np}, v_{np}, p_{np}, T_{np} (see (12)), and the explicit form of small perturbations U^*, T^*, V^{II} (describing a laminar flow along the irregularity) will be given below.

This choice of initial data (16)–(18) actually means that we will investigate unsteady disturbances of the flow caused by the presence of the heated irregularity, assuming that the main flow is a steady-state flow with the Blasius velocity profile and the corresponding temperature profile (14), (15).

As a result of the above described actions, we obtain the following result.

Theorem 1 *The formal asymptotic solution of problem (1)–(6), (16)–(18) has the form*

$$u(t, x, z) = f'\big(\tau/\sqrt{x}\big) + \varepsilon^{1/3}\big(h(\xi)f''(\tau) + u^{\mathrm{I}}_1(t, \xi, \theta)\big) + O(\varepsilon^{2/3}), \tag{19}$$
$$v(t, x, z) = \varepsilon^{2/3}\big(v^{\mathrm{II}}_2(t, \xi, \tau) + v^{\mathrm{I}}_2(t, \xi, \theta)\big) + O(\varepsilon), \tag{20}$$
$$p(t, x, z) = p_\infty + \varepsilon^{2/3}p^{\mathrm{II}}_2(t, \xi, \tau) + O(\varepsilon), \tag{21}$$
$$T(t, x, z) = 1 + g(\tau/\sqrt{x})(\overline{T} - 1) + q(\tau/\sqrt{x}) + T^{\mathrm{I}}_0(t, \xi, \theta) + O(\varepsilon^{1/3}), \tag{22}$$

where $\tau = z\varepsilon^{-1}$, $\theta = z\varepsilon^{-4/3}$, $z = y - y_s$, $\xi = (x - 1)\varepsilon^{-1}$, $f(\gamma)$ is the Blasius function (13), and the functions $g(\gamma)$ and $q(\gamma)$ are solutions of problems (14), (15). The functions $u^{\mathrm{I}}_1(t, \xi, \theta)$, $v^{\mathrm{I}}_2(t, \xi, \theta)$, and $T^{\mathrm{I}}_0(t, \xi, \theta)$ are determined by the relations

$$u^*_1 = u^{\mathrm{I}}_1 + \big(\theta + h(\xi)\big)f''(0), \quad v^*_2 = v^{\mathrm{I}}_2 + v^{\mathrm{II}}_2\big|_{\tau=0}, \quad T^*_0 = 1 + g(0)(\overline{T} - 1) + T^{\mathrm{I}}_0, \tag{23}$$

where the functions $u_1^*(t,\xi,\theta)$, $v_2^*(t,\xi,\theta)$ and $T_0^*(t,\xi,\theta)$ are solutions of of the initial-boundary value problem for the Prandtl system of equations with self-induced pressure

$$\frac{\partial u_1^*}{\partial t}+u_1^*\left(\frac{\partial u_1^*}{\partial \xi}-h'(\xi)\frac{\partial u_1^*}{\partial \theta}\right)+v_2^*\frac{\partial u_1^*}{\partial \theta}=-\frac{\partial p_2^{\mathrm{II}}}{\partial \xi}\bigg|_{\tau=0}+\frac{\partial^2 u_1^*}{\partial \theta^2}, \tag{24}$$

$$\frac{\partial v_2^*}{\partial \theta}+\frac{\partial u_1^*}{\partial \xi}-h'(\xi)\frac{\partial u_1^*}{\partial \theta}=0, \tag{25}$$

$$\frac{\partial T_0^*}{\partial t}+u_1^*\left(\frac{\partial T_0^*}{\partial \xi}-h'(\xi)\frac{\partial T_0^*}{\partial \theta}\right)+v_2^*\frac{\partial T_0^*}{\partial \theta}=\frac{1}{\mathrm{Pr}}\frac{\partial^2 T_0^*}{\partial \theta^2}, \tag{26}$$

$$u_1^*\big|_{\theta=0}=v_2^*\big|_{\theta=0}=0,\ \frac{\partial u_1^*}{\partial \theta}\bigg|_{\theta\to\infty}=f''(0),\ u_1^*\big|_{\xi\to\pm\infty}=\theta f''(0), \tag{27}$$

$$v_2^*\big|_{\xi\to\pm\infty}=0,\ T_0^*\big|_{\theta=0}=\overline{T}+T_\Gamma(\xi),\ T_0^*\big|_{\theta\to\infty}=\overline{T},\ T_0^*\big|_{\xi\to\pm\infty}=\overline{T}, \tag{28}$$

$$u_1^*\big|_{t=0}=U^*(\xi,\theta),\quad T_0^*\big|_{t=0}=T^*(\xi,\theta), \tag{29}$$

where U^*, T^* are some smooth functions. The function v_2^{II} is the solution of the initial-boundary value problem for the Rayleigh-type equation

$$\varepsilon^{1/3}\frac{\partial}{\partial t}\int_{-\infty}^{\xi}\Delta_{\xi',\tau}v_2^{\mathrm{II}}\,d\xi'+f'(\tau)\Delta_{\xi,\tau}v_2^{\mathrm{II}}-f'''(\tau)v_2^{\mathrm{II}}=0,$$

$$v_2^{\mathrm{II}}\big|_{\tau=0}=v_2^*\big|_{\theta\to\infty},\quad v_2^{\mathrm{II}}\big|_{\tau\to\infty}=0,\quad v_2^{\mathrm{II}}\big|_{\xi\to\pm\infty}=0,\quad v_2^{\mathrm{II}}\big|_{t=0}=V^{\mathrm{II}}(\xi,\tau), \tag{30}$$

where $\Delta_{\xi,\tau}=\frac{\partial^2}{\partial\xi^2}+\frac{\partial^2}{\partial\tau^2}$ and $V_2(\xi,\tau)$ is some smooth function (e.g., $V^{\mathrm{II}}=e^{-\tau}v_2^*\big|_{\theta\to\infty}$). The function $p_2^{\mathrm{II}}(t,\xi,\tau)$ is determined from the relation

$$\frac{\partial p_2^{\mathrm{II}}}{\partial \xi}=\varepsilon^{1/3}\frac{\partial}{\partial t}\int_{-\infty}^{\xi}\frac{\partial v_2^{\mathrm{II}}}{\partial \tau}\,d\xi'+f'(\tau)\frac{\partial v_2^{\mathrm{II}}}{\partial \tau}-f''(\tau)v_2^{\mathrm{II}}$$

with the boundary condition $p_2^{\mathrm{II}}\big|_{\xi\to-\infty}=0$.

Remark 1 The expression for the self-induced pressure in equation (24) can be written as (see [14,17,18])

$$\frac{\partial p_2^{\mathrm{II}}}{\partial \xi}\bigg|_{\tau=0}=-f''(0)v_2^*\big|_{\theta\to\infty}, \tag{31}$$

which allows modeling the flow in the lower deck (i.e., solving problem (24)–(29)) without solving the problem for the Rayleigh-type equation (30).

Proof As was noted above, the hydrodynamic part of this theorem (i.e., the derivation of equations describing the flow velocities and pressure (19)–(21) in the layers of the double-deck structure) was proved earlier, see [13]. Here we restrict ourselves only to the derivation of equations describing the temperature distribution. Acting according to the algorithm described above, we substitute expansion (10) with the already found velocities and pressure (19)–(21) into equation (4). Note that $f'(\tau/\sqrt{x})=\mathrm{u}_0^{\mathrm{II}}+1$ and $u_1^{\mathrm{II}}=h(\xi)f''(\tau)$.

Our goal is to obtain the main terms of the expansion for the temperature (see (22)), i.e., we want to obtain equations for T_0^{II} and T_0^{I}. So we obtain equations in the middle deck region II by letting $\theta\to\infty$ in the equations obtained after substituting expansions (10), (19)–(21) into equation (4). At ε^0 we have the following equation:

$$\varepsilon^{-2/3}\frac{\partial T_0^{\mathrm{II}}}{\partial t}+\left(u_0^{\mathrm{II}}+1\right)\frac{\partial T_0^{\mathrm{II}}}{\partial x}+\left(v_3^{\mathrm{II}}+v_3^{\mathrm{ext}}\big|_{z=0}\right)\frac{\partial T_0^{\mathrm{II}}}{\partial \tau}+v_2^{\mathrm{II}}\frac{\partial T_1^{\mathrm{II}}}{\partial \tau}+u_1^{\mathrm{II}}\left(\frac{\partial T_2^{\mathrm{II}}}{\partial \xi}-h'(\xi)\frac{\partial T_1^{\mathrm{II}}}{\partial \tau}\right)+$$
$$+(1+u_0^{\mathrm{II}})\left(\frac{\partial T_3^{\mathrm{II}}}{\partial \xi}-h'(\xi)\frac{\partial T_2^{\mathrm{II}}}{\partial \tau}\right)-\frac{1}{\mathrm{Pr}}\frac{\partial^2 T_0^{\mathrm{II}}}{\partial \tau^2}=\mathrm{Ec}\left(\frac{\partial u_0^{\mathrm{II}}}{\partial \tau}\right)^2.$$

Passing to the limit as $\xi \to -\infty$ in this equation, and taking into account that, according to the localization principle (see (11)), $T_i^{\mathrm{II}}\big|_{\xi\to-\infty} = 0$, $i = 1, 2$, $T_3^{\mathrm{II}}\big|_{\xi\to-\infty} \to T_{3,np}^{\mathrm{II}}(t, x, \tau)$, $v_2^{\mathrm{II}}\big|_{\xi\to-\infty} = 0$, $v_3^{\mathrm{II}}\big|_{\xi\to-\infty} + v_3^{\mathrm{ext}}\big|_{z=0} = v_{3,np}(x, \tau)$ (see (12)), and $u_0^{\mathrm{II}} = f'(\tau/\sqrt{x}) - 1$, we obtain the following equation:

$$\varepsilon^{-2/3}\frac{\partial T_0^{\mathrm{II}}}{\partial t} + f'(\tau/\sqrt{x})\frac{\partial T_0^{\mathrm{II}}}{\partial x} + \frac{1}{2\sqrt{x}}\big(f'(\tau/\sqrt{x})\frac{\tau}{\sqrt{x}} - f(\tau/\sqrt{x})\big)\frac{\partial T_0^{\mathrm{II}}}{\partial \tau} - \\ -\frac{1}{\mathrm{Pr}}\frac{\partial^2 T_0^{\mathrm{II}}}{\partial \tau^2} = \mathrm{Ec}\left(\frac{f''(\tau/\sqrt{x})}{\sqrt{x}}\right)^2. \tag{32}$$

Obviously, if we consider the Cauchy problem for this equation with initial condition (18), then the solution at small times $\varepsilon^{2/3}t$ has the form

$$T_0^{\mathrm{II}} = T_{0,nps}^{\mathrm{II}} + O(\varepsilon^{2/3}) = g(\tau/\sqrt{x})(\overline{T} - 1) + q(\tau/\sqrt{x}) + O(\varepsilon^{2/3}),$$

where the function $g(\gamma)$ is the stationary solution of equation (32) with zero right-hand side and nonzero boundary conditions and the function $q(\gamma)$ is the stationary solution of equation (32) with nonzero right-hand side and zero boundary conditions, see (14), (15).

Now we consider the temperature distribution in the lower deck region I. At $\varepsilon^{-2/3}$ we have the equation

$$\frac{\partial T_0^{\mathrm{I}}}{\partial t} + \theta\frac{\partial u_0^{\mathrm{II}}}{\partial \tau}\Big|_{\tau=0}\left(\frac{\partial T_0^{\mathrm{I}}}{\partial \xi} - h'(\xi)\frac{\partial T_0^{\mathrm{I}}}{\partial \theta}\right) + (v_2^{\mathrm{I}} + v_2^{\mathrm{II}}\big|_{\tau=0})\frac{\partial T_0^{\mathrm{I}}}{\partial \theta} + \\ + (u_1^{\mathrm{I}} + u_1^{\mathrm{II}}\big|_{\tau=0})\left(\frac{\partial T_0^{\mathrm{I}}}{\partial \xi} - h'(\xi)\frac{\partial T_0^{\mathrm{I}}}{\partial \theta}\right) = \frac{1}{Pr}\frac{\partial^2 T_0^{\mathrm{I}}}{\partial \theta^2}.$$

Passing to the functions u_1^*, v_2^* and T_0^* according to formulas (23), we obtain equation (26).

It remains to obtain the boundary conditions. Substituting expansion (10) into boundary condition (6) for the temperature and taking the results obtained above into account, at ε^0 we obtain:

$$1 + T_0^{\mathrm{II}}\big|_{\tau=0} + T_0^{\mathrm{I}}\big|_{\theta=0} = \overline{T} + T_\Gamma(\xi). \tag{33}$$

The left-hand side of this equality is equal to $T_0^*\big|_{\theta=0}$, i.e., we obtain the boundary condition $T_0^*\big|_{\theta=0} = \overline{T} + T_\Gamma(\xi)$. Passing to the limit as $\xi \to -\infty$ in (33) and taking into account the fact that $T_\Gamma(-\infty) = 0$ due to the statement of the problem, we have

$$1 + T_0^{\mathrm{II}}\big|_{\tau=0} = \overline{T},$$

whence, after substituting the explicit form T_0^{II}, we obtain the condition $g(0) = 1$.

By letting $\theta \to \infty$ in expression (23) for T_0^*, we obtain the boundary condition $T_0^*\big|_{\theta\to\infty} = 1 + g(0)(\overline{T} - 1) = \overline{T}$ using the definition of the boundary layer function: $T_0^{\mathrm{I}}\big|_{\theta\ to\infty} = 0$. Similar conditions are obtained as $\xi \to \pm\infty$. □

4 Numerical simulation of heat transfer near streamlined surface

Now we consider the numerical simulation of heat transfer in the region near the irregularity, i.e., in the lower deck of the double-deck structure (see region I in Fig. 1). The flow[3] and the temperature distribution in this region are described by system (24)–(29), (31) which we will solve numerically. This system can be efficiently solved numerically by using difference schemes, and we will use the explicit first-order (for all variables) difference scheme due to its simple and efficient parallelization capability for computing on both modern multi-core CPU and GPU (we use NVIDIA CUDA[4] technology) due to their availability on modern personal computers. We once again emphasize that our approach does not require the use of high-performance clusters. Here we will not present the difference scheme due to its triviality.

[3] By the flow in this section we mean only the velocity field

[4] https://developer.nvidia.com/cuda-zone

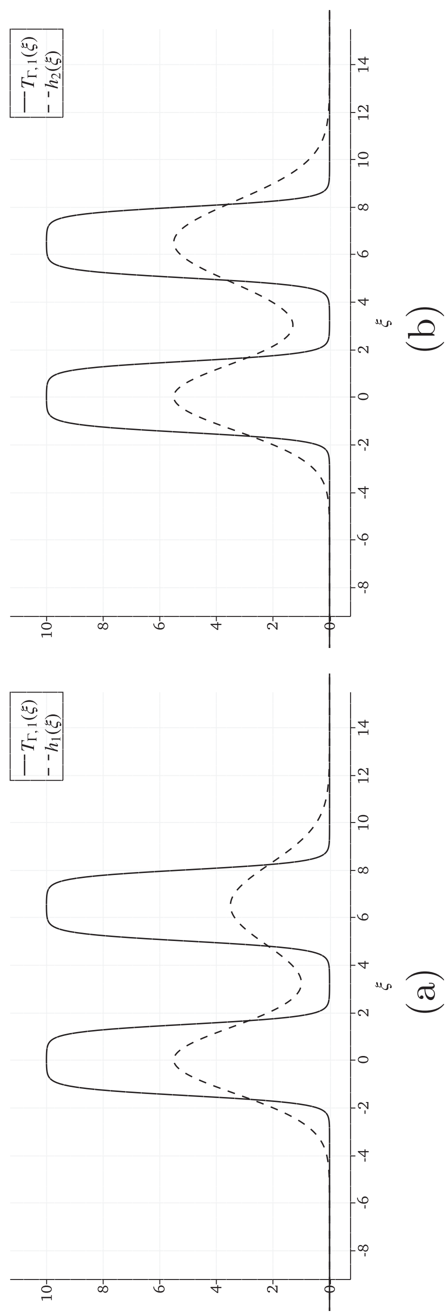

Fig. 2 Functions describing the irregularities (dashed curves) and the function $T_{\Gamma,1}(\xi)$ describing the surface heating (solid curve): (a) $h_1(\xi)$; (b) $h_2(\xi)$

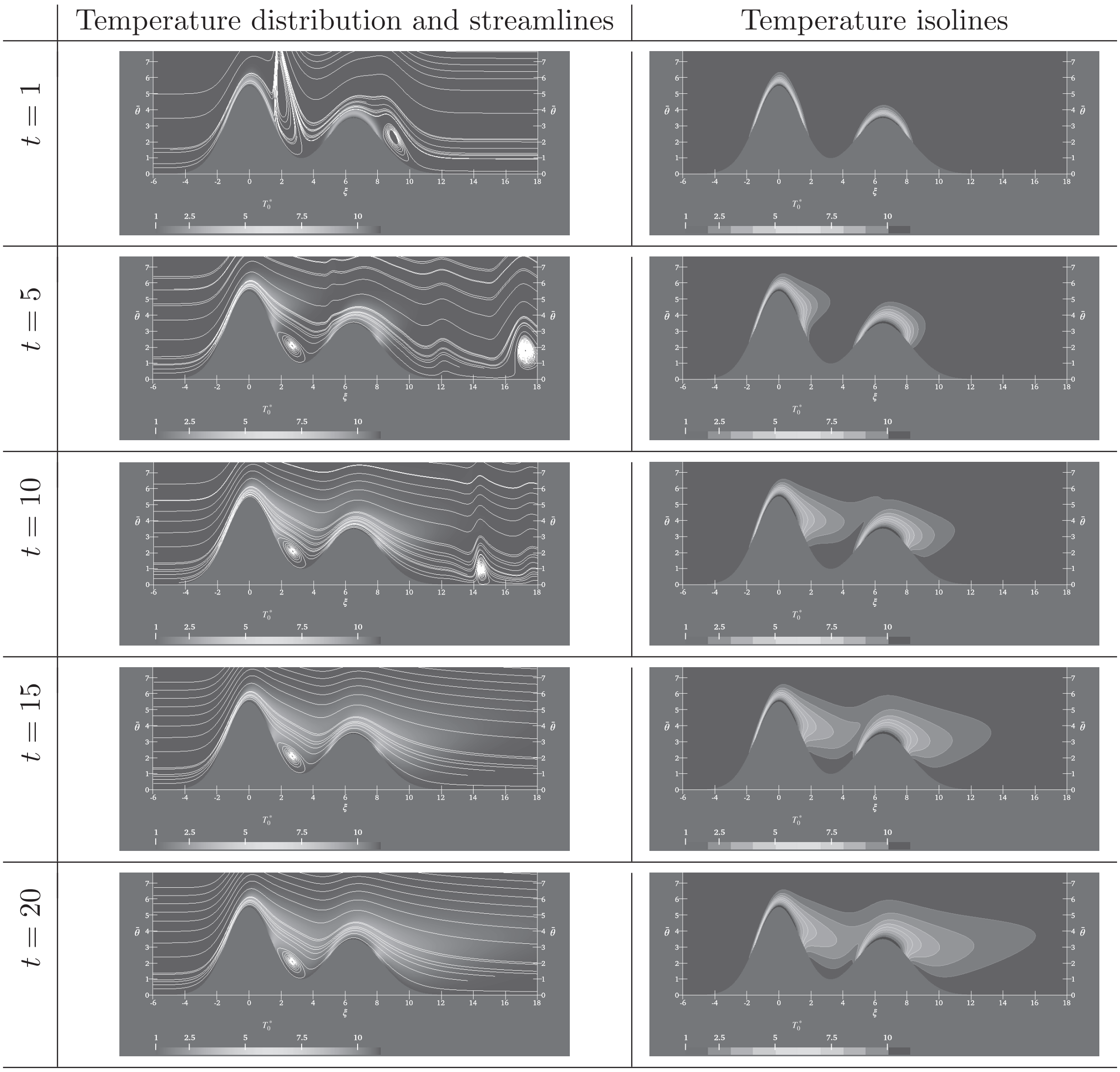

Fig. 3 Temperature distribution and streamlines at different times t for the irregularity shape $h_1(\xi)$ (see (37)) and the function $T_{\Gamma,1}(\xi)$ (see (38)) describing the surface heating, $\mathrm{Pr} = 10$

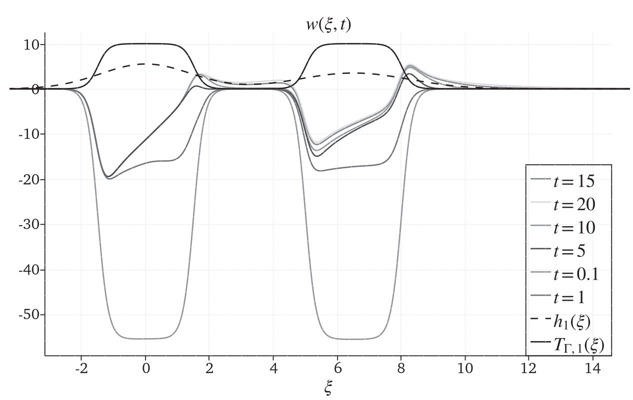

Fig. 4 The surface heat flux $w(\xi, t)$ at different times t (colored curves) with the irregularity shape $h_1(\xi)$ (dashed black curve) and the function $T_{\Gamma,1}(\xi)$ (see (38)) describing the surface heating (solid black curve), $\mathrm{Pr} = 10$

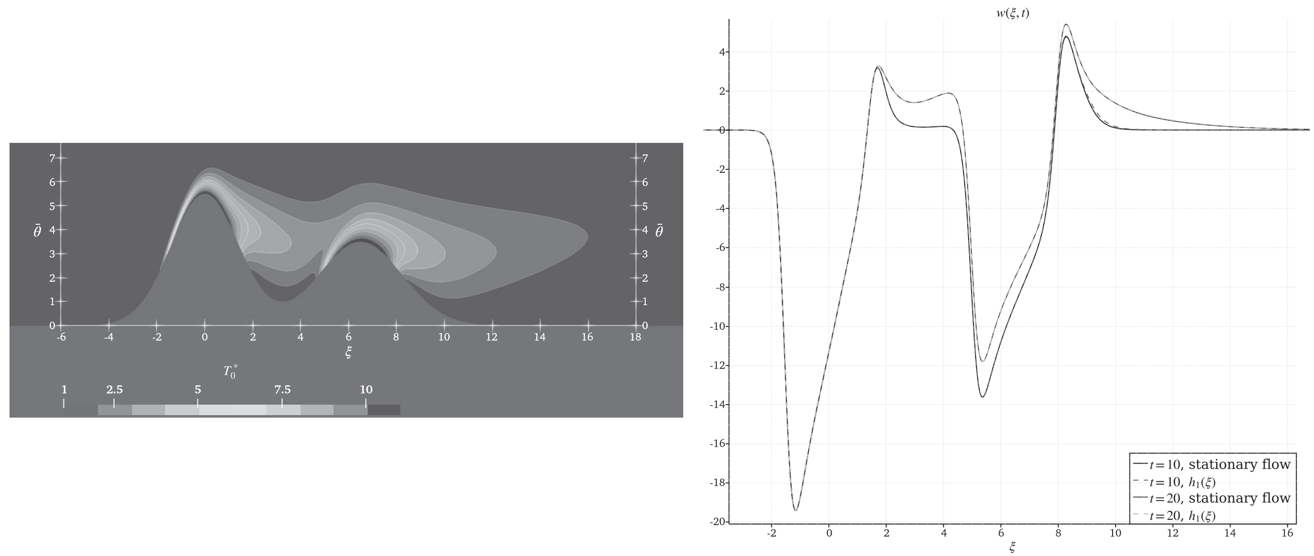

(a) (b)

Fig. 5 Influence of the process of establishment of the stationary flow on the heat transfer: (a) — the temperature isolines at time $t = 20$, the heating is turned on after after the flow has reached the steady state; (b) — plots of the surface heat flux $w(\xi, t)$ at times $t = 10$ and $t = 20$: dotted curves — at the start of the surface heating immediately after the beginning of the simulation, solid curves — at the start of the surface heating after the flow has reached the steady state; the time t is counted from the time of the beginning of the surface heating; both illustrations are for the irregularity shape $h_1(\xi)$ (see (37)) and the function $T_{\Gamma,1}(\xi)$ (see (38)) describing the surface heating, $\mathrm{Pr} = 10$

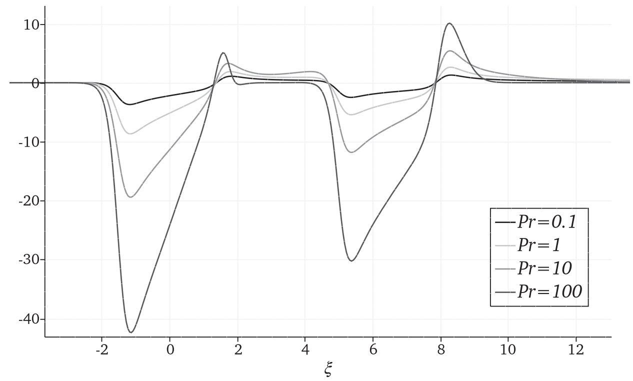

Fig. 6 Plots of the function $w(\xi, t)$ at time $t = 20$ for different values of the Prandtl number Pr for the irregularity shape $h_1(\xi)$ (see (37)) and the function $T_{\Gamma,1}(\xi)$ (see (38)) describing the surface heating

The parameters used for numerical simulation are as follows: the spatial domain in which the simulation is performed:

$$\Omega = \{-50 \le \xi \le 50;\ 0 \le \theta \le 100\},$$

the simulation time: $0 \le t \le 20$, the difference scheme steps: $h_\xi = h_\theta = 10^{-2}$, $h_t = 10^{-4}$. Note that the error due to cutoff of the original unbounded domain $\hat{\Omega} = \{\xi \in \mathbb{R},\ \theta \in \mathbb{R}^+\}$ will be quite small (of the same order as the difference scheme approximation error, see [13–15,22–24]).

We chose the following initial data for problem (24)–(29), (31):

$$u_1^*\big|_{t=0} = U^* = \begin{cases} f''(0)\theta(1+0.2h(\xi)), & \theta \le 5, \\ f''(0)(\theta + h(\xi)), & \theta > 5, \end{cases} \qquad T_0^*\big|_{t=0} = T^* = \overline{T} \tag{34}$$

(the laminar initially flow around the irregularity at constant temperature)

Note that the hydrodynamic part of the problem (i.e., the velocity field) has already been studied numerically earlier, see [13–15]. In these papers was obtained that problem (24), (25), (27), (29), (31), (34) has a stationary solution but the behavior of the flow depends on the geometry of the irregularity. For example, if we consider a hump-like irregularity in the form $h(\xi) = Ae^{-\xi^2/4}$ (where $A = \text{const}$), then there exists a critical value of the amplitude A^*. If $A < A^*$, then the flow is laminar and becomes stationary after some time from the beginning of the simulation. If $A > A^*$, then we observed the phenomenon of boundary layer separation which occurs in it with the formation of a vortex zone, and this flow is also stationary (starting after some time t^* from the beginning of the simulation). The situation in both cases is shown in the left column in Fig. 3: the amplitude of the left hump is greater than the critical one, and the amplitude of the right one is less, and we observe a stationary vortex behind the left hump. In Fig. 7 (a)–(f), both humps have the same amplitude greater than the critical one, and we observe two zones of boundary layer separation behind the humps.

In this paper, we will focus on the study of heat transfer. Note that all figures below are made in coordinates with a curvilinear boundary, $(\theta + \mu, \xi) \overset{\text{def}}{=} (\bar{\theta}, \xi)$; the color in them shows the temperature, and the white lines are streamlines. All calculations were carried out in the Ω-region, and the figures below show a part of this region that is of interest. The visualization of the calculation results was carried out in the ParaView[5] program.

We also note that one of the possible applications of the considered mathematical model is the modeling of the heat removal from small devices. In this regard, the value of the heat flux from the streamlined surface is of interest:

$$\begin{aligned} Q &= -\lambda \frac{\partial T}{\partial \mathbf{n}}\bigg|_{z=0} = -\lambda \left[\frac{1}{\varepsilon} \frac{\partial T_0^{\mathrm{II}}}{\partial \tau}\bigg|_{\tau=0} + \frac{1}{\varepsilon^{4/3}} \frac{\partial T_0^{\mathrm{I}}}{\partial \theta}\bigg|_{\theta=0} \right] \\ &= -\lambda \left[\frac{1}{\varepsilon} \frac{g'(0)}{\sqrt{x}} + \frac{1}{\varepsilon} \frac{q'(0)}{\sqrt{x}} + \frac{1}{\varepsilon^{4/3}} w(\xi, t) \right], \end{aligned} \tag{35}$$

[5] https://www.paraview.org/

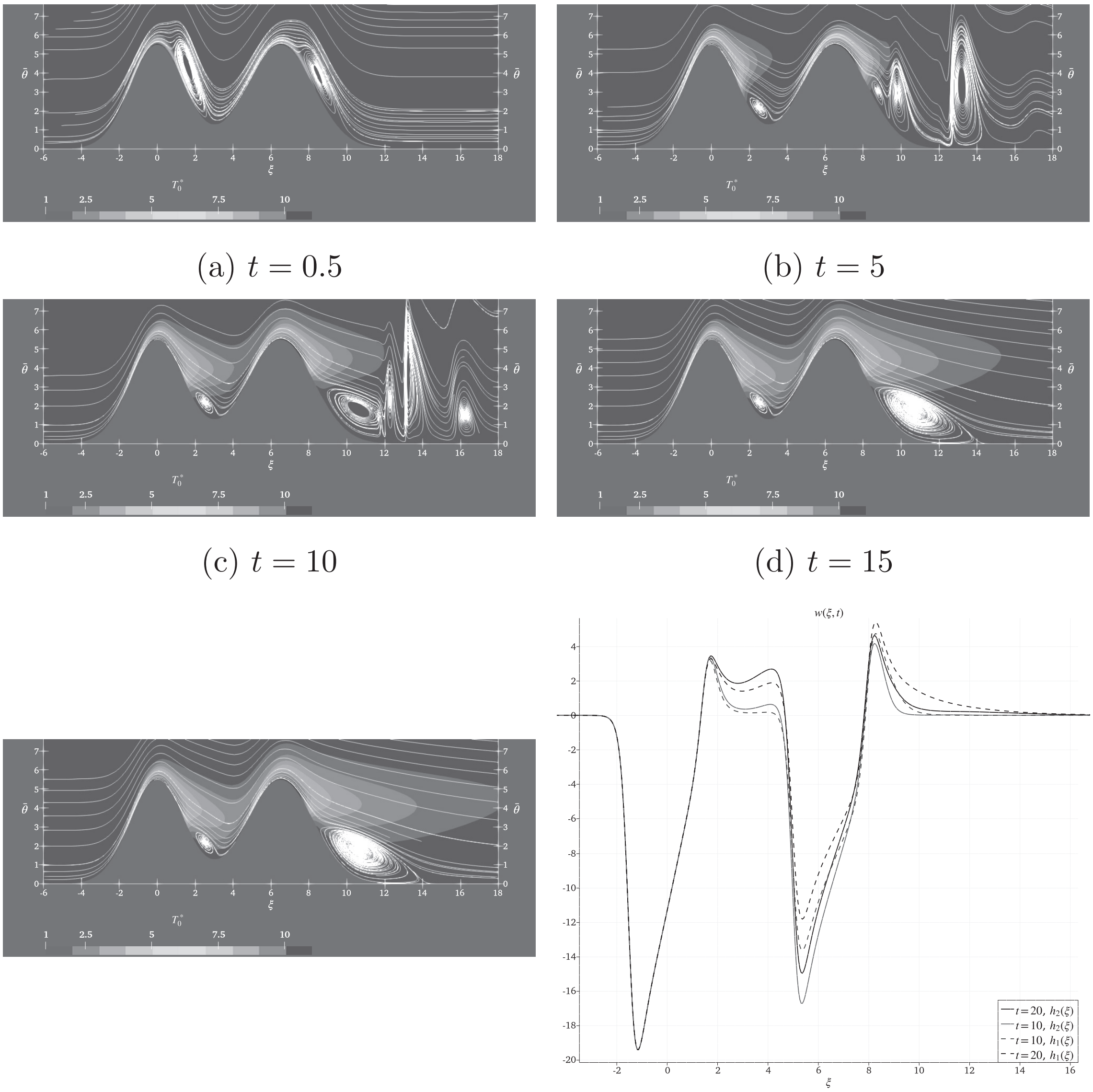

(a) $t = 0.5$ (b) $t = 5$

(c) $t = 10$ (d) $t = 15$

(e) $t = 20$ (f) $w(\xi, t)$

Fig. 7 Influence of the hump amplitude and the presence of a vortex on heat transfer: (a)–(e) — the temperature isolines and streamlines at different times t with the irregularity shape $h_2(\xi)$ (see (39)) and the function $T_{\Gamma,1}(\xi)$ (see (38)) describing the surface heating; (f): comparison of the plots of the function $w(\xi, t)$ (surface heat flux) for the irregularities of the shapes $h_1(\xi)$ (dashed curve) and $h_2(\xi)$ (solid curve) at the time $t = 10$ (blue curves) and $t = 20$ (black curves); Pr = 10

where $\lambda = \hat{k}\hat{T_\infty}/\hat{x_0}$ (see Section 2) and

$$w(\xi, t) \stackrel{\text{def}}{=} \left.\frac{\partial T_0^{\mathrm{I}}}{\partial \theta}\right|_{\theta=0} = \left.\frac{\partial T_0^*}{\partial \theta}\right|_{\theta=0}. \tag{36}$$

The first two terms $g'(0)$ and $q'(0)$ in formula (35) are known (including their dependence on the parameters of the problem, i.e., the Prandtl Pr and Eckert Ec numbers), see [20,21], and the more significant term $w(\xi, t)$ will be illustrated in figures below.

Now we consider the results of the simulation. Let the Prandtl number Pr $= 10$. First, we consider the following form of the irregularity

$$h_1(\xi) = 5.5e^{-\xi^2/4} + 3.5e^{-(\xi-6.5)^2/6}. \tag{37}$$

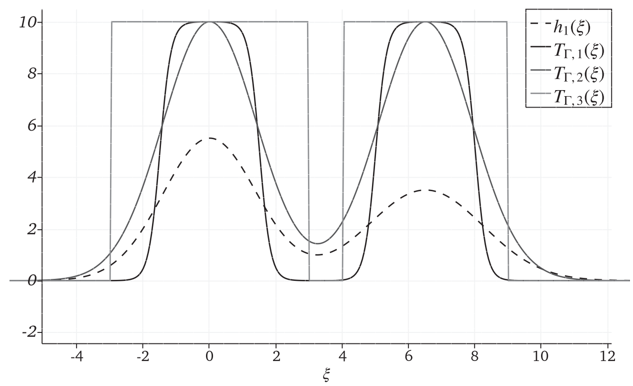

Fig. 8 Function $h_1(\xi)$ (see (37)) describing the shape of the irregularity (dashed curve) and the functions $T_{\Gamma,i}(\xi)$, $i = 1, 2, 3$ (see (38) and (40)) describing the surface heating (solid curves)

These are two closely spaced humps of different amplitude and width, see Fig. 2 (a). Note that the amplitude of the left hump is $A = 5.5 > A^*$ and the amplitude of the right hump is $A = 3.5 < A^*$. Let the temperatures of the surface and the main flow be equal, i.e., let $\overline{T} = 1$, and let the temperature of the irregularity (the function T_Γ describing the local heating) be of the form

$$T_{\Gamma,1}(\xi) = 5\big(\tanh\big(3(1.5 - x)\big)\tanh\big(3(1.5 + x)\big) + \\ + \tanh\big(3(1.5 - (x - 6.5))\big)\tanh\big(3(1.5 + (x - 6.5))\big) + 2\big), \tag{38}$$

see Fig. 2 (a). Note that the function (38) is chosen so that the main heating occurs approximately in the upper half of the hump.

The simulation results for the irregularity form $h_1(\xi)$ and the temperature $T_{\Gamma,1}$ are presented in Figs. 3 and 4. The left column in Fig. 3 illustrates the process of formation of the stationary flow, i.e., a laminar flow with the vortex behind the left hump (see the streamlines). The right column in Fig. 3 shows the corresponding temperature isolines. It can be seen that the fluid flow is heated from the irregularity at a time after the beginning of the simulation (see $t = 1$). After that, the heated flow begins to drift along another flow (there are more flow velocities at the top), see $t = 5$ (the flow is directed from left to right), and the heated fluid propagates in the right direction (see $t = 10$, $t = 15$, $t = 20$). Note that the presence of the vortex has some small effect on the flow, see $t = 5$.

Now we consider the heat flux from the surface, i.e., the function $w(\xi, t)$ (see (36)) for the irregularity form $h_1(\xi)$ and the temperature $T_{\Gamma,1}$. It can be seen in Fig. 4 that the range of the function $w(\xi, t)$ decreases rather fast in time from the initial state, and we can say that it practically comes to the steady state near the left hump at $t = 5$. We also observe the appearance of small zones behind the humps in which the function $w(\xi, t)$ has a different sign (in practical application, this means that the local heating can occur in this area), and this zone is larger behind the right hump.

Note that the process of coming to the stationary flow does not affect the temperature some time after the beginning of the simulation, i.e., if we turn on the heating of the irregularity after the flow has reached the steady state, then the result will be exactly the same, see Fig. 5.

Now let us study the influence of the Prandtl number Pr on the heat removal from the surface (i.e., on the form of the function $w(\xi, t)$). The plots of the surface heat flux function $w(\xi, t)$ are shown in Fig. 6 at time $t = 20$. It can be seen that the plots have a similar structure, the values of the extrema differ significantly (approximately by two times), and their coordinates differ slightly. In general, these results are expected from the form of equation (26). Namely, the smaller the Prandtl number, the larger the coefficient multiplying the second derivative and, accordingly, the rate of the heating of the fluid layer near the surface, which naturally leads to a smaller temperature gradient near the surface.

Now we consider two irregularities with the same amplitude (see Fig. 2 (b)):

$$h_2(\xi) = 5.5e^{-\xi^2/4} + 5.5e^{-(\xi - 6.5)^2/6}, \tag{39}$$

$A = 5.5 > A^*$, and we choose the same function describing the heating of the surface — $T_{\Gamma,1}(\xi)$ (see (38)). The simulation results for this case are shown in Fig. 7. The comparison of the temperature isolines with the

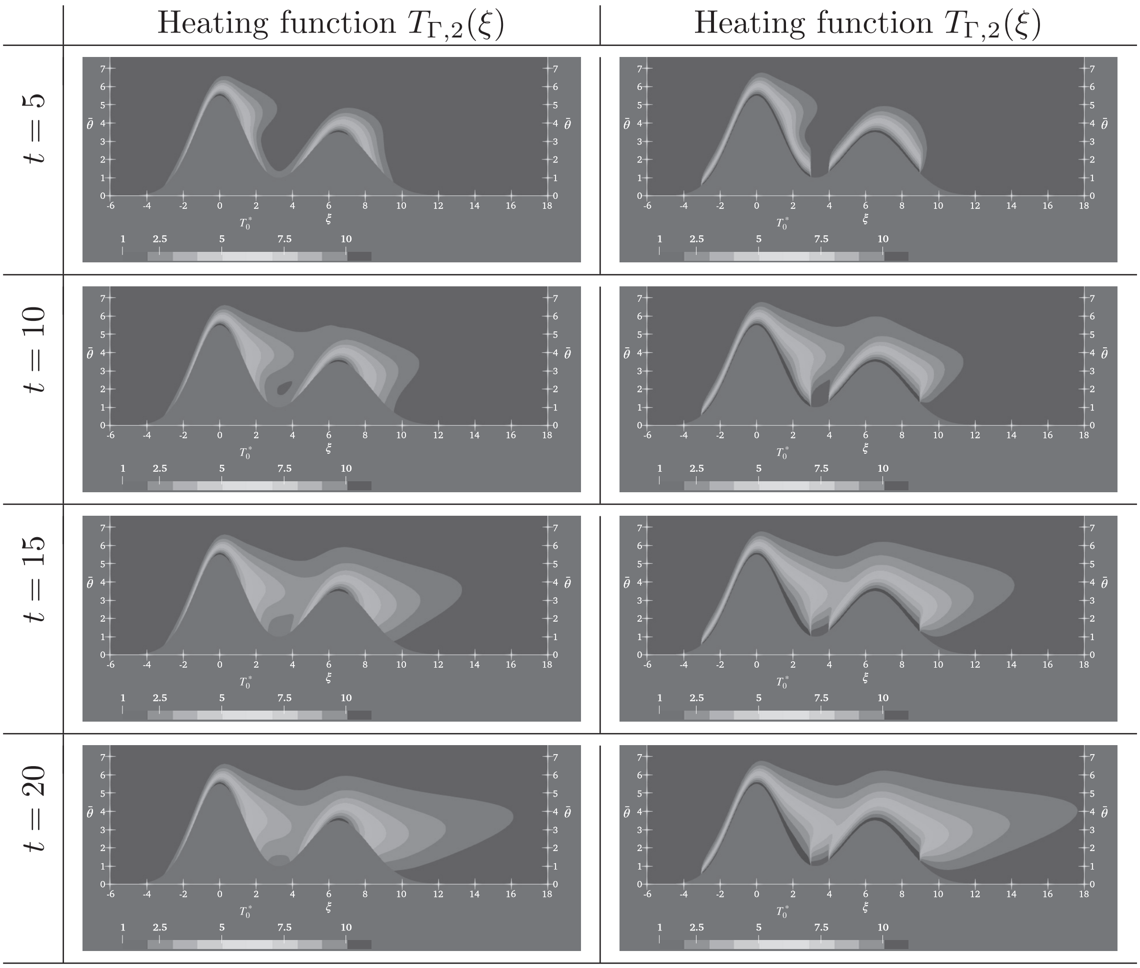

Fig. 9 Temperature isolines at different times t for the irregularity shape $h_1(\xi)$ (see (37)) and the functions $T_{\Gamma,2}(\xi)$, $T_{\Gamma,3}(\xi)$ (see (40)) describing the surface heating; $\mathrm{Pr} = 10$

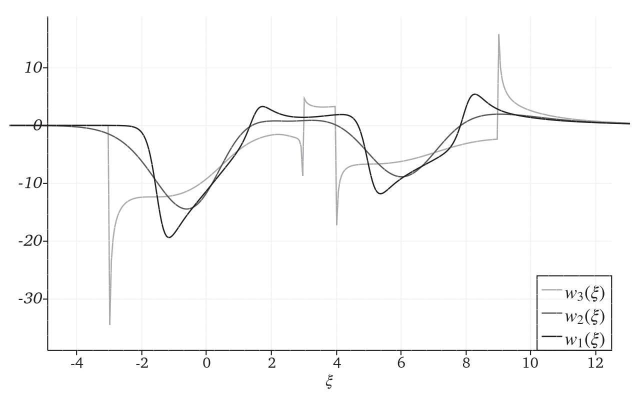

Fig. 10 Functions $w_i(\xi, 20)$ (surface heat fluxes) corresponding to the functions $T_{\Gamma,i}(\xi)$, $i = 1, 2, 3$, with the irregularity shape $h_1(\xi)$; $\mathrm{Pr} = 10$

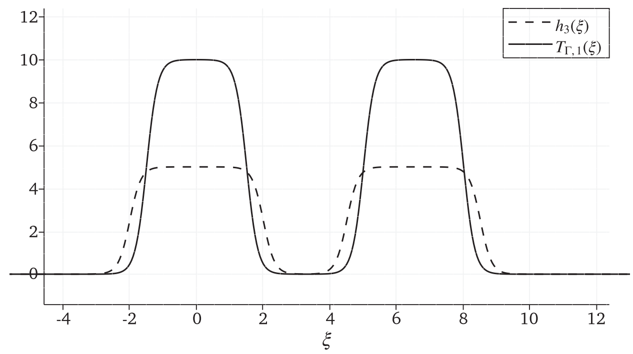

Fig. 11 Irregularity shape $h_3(\xi)$ (see (41)) and the heating function $T_{\Gamma,1}(\xi)$ (see (38))

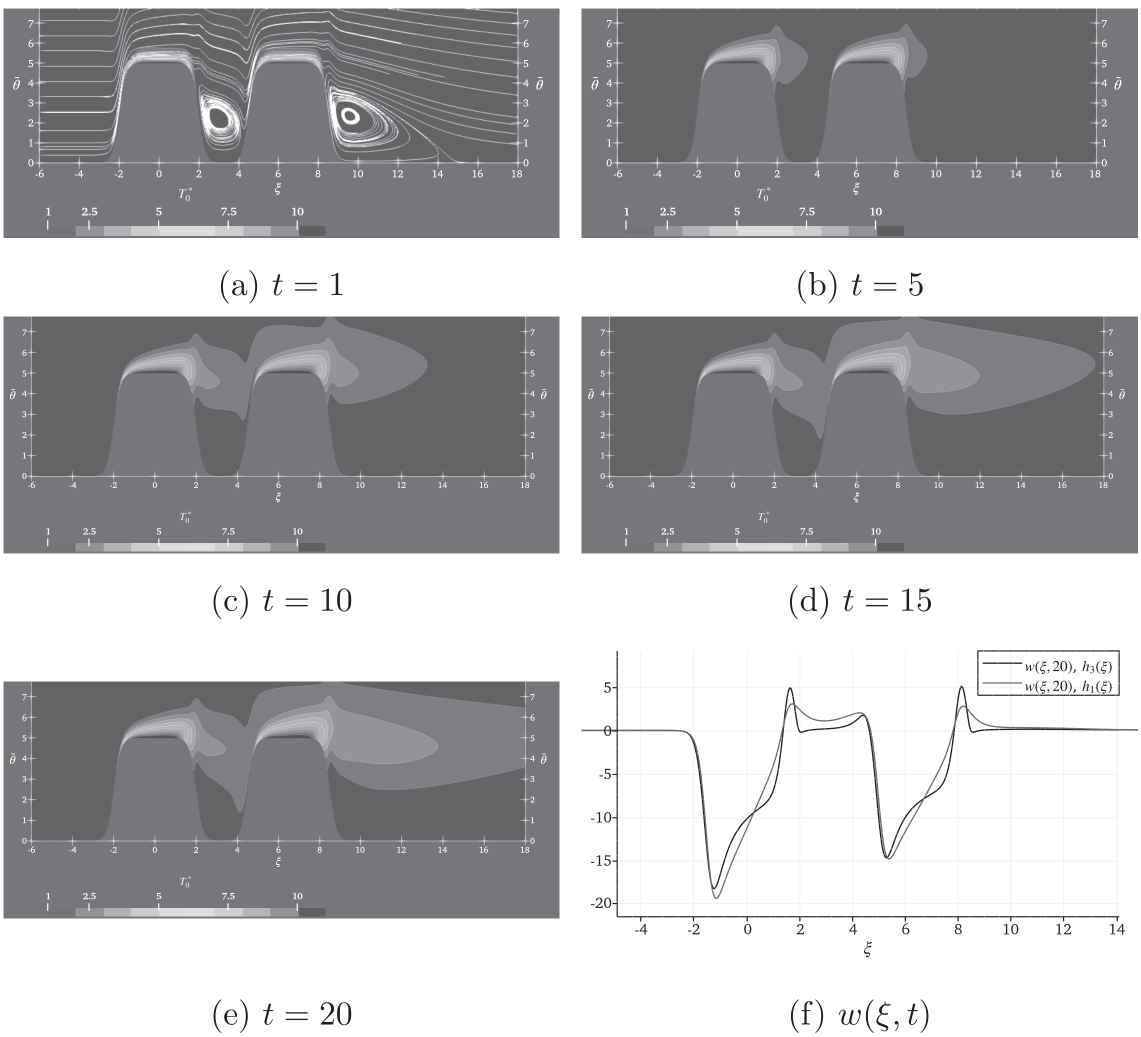

(a) $t = 1$ (b) $t = 5$

(c) $t = 10$ (d) $t = 15$

(e) $t = 20$ (f) $w(\xi, t)$

Fig. 12 Temperature distribution for the irregularity shape $h_3(\xi)$ and the function $T_{\Gamma,1}(\xi)$ describing the surface heating: (a) — streamlines of the stationary flow; (a)–(e) — the temperature isolines at different times t; (f): comparison of the plots of the function $w(\xi, t)$ for the irregularity shapes $h_2(\xi)$ (red curve) and $h_3(\xi)$ (black curve) at time t =20; Pr = 10

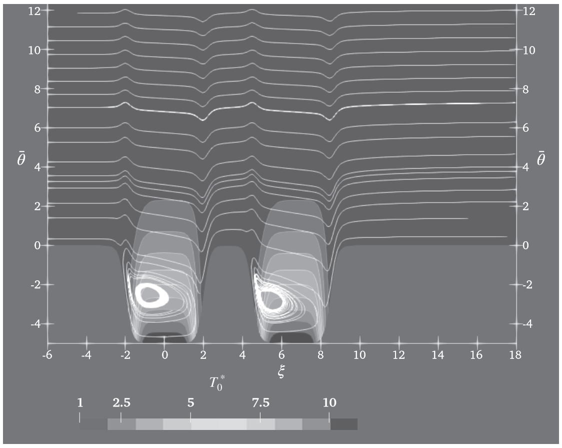

(a) $t = 1$

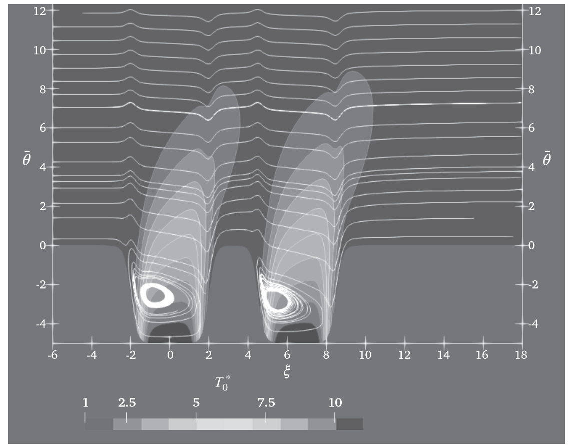

(b) $t = 5$

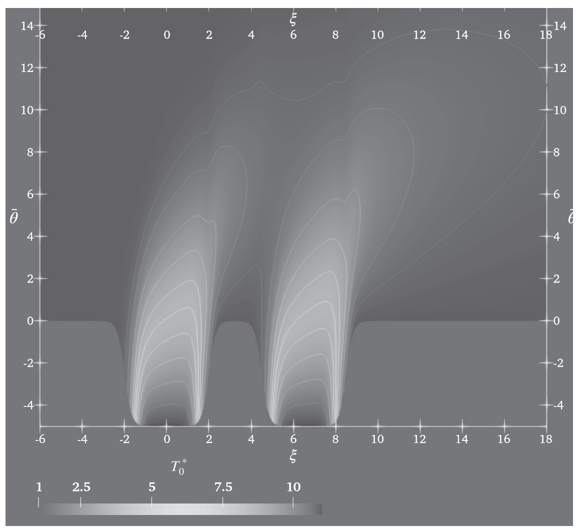

(c) $t = 10$

Fig. 13 Streamlines of the stationary flow (a), (b) and the temperature isolines (a)–(c) at different times t with the irregularity shape $h_4(\xi) = -h_3(\xi)$ and the function $T_{\Gamma,1}(\xi)$ describing the heating; Pr $= 0.1$

case $h_1(\xi)$ (see fig. 3) shows that small changes in the temperature distribution begin in the flow behind the first hump, and the largest difference in the heat flux from the surface (see Fig. 7 (e)) is concentrated near the top of the second hump and behind it (this is indicated by the presence of the second zone of the boundary layer separation).

Now let us study the influence of the function describing the heating of the surface on the heat transfer. We consider functions with smaller and larger localization of the region of maximal heating:

$$T_{\Gamma,2}(\xi) = 10\big(e^{-\xi^2/4} + e^{-(\xi-6.5)^2/4}\big),\ T_{\Gamma,3}(\xi) = \begin{cases} 10, & \xi \in (-3, 3) \cup (4, 9) \stackrel{\text{def}}{=} I, \\ 0, & \xi \in [-50, 50] \setminus I, \end{cases} \tag{40}$$

see Fig. 8.

The simulation results for the irregularity shape $h_1(\xi)$ (see (37)) and for the functions $T_{\Gamma,2}(\xi)$ and $T_{\Gamma,3}(\xi)$ are shown in Fig. 9, and for $T_{\Gamma,1}$, in Fig. 3 (see the second column). The comparison of the temperature isolines in Figs. 3 and 9 showed that the isolines for the cases $T_{\Gamma,1}$ and $T_{\Gamma,2}$ are arranged similarly, but the case $T_{\Gamma,2}$ is characterized by a greater heating of the region between the humps. In the case of the piecewise-constant function $T_{\Gamma,3}$, the heating value and the rate are noticeably greater, but there is still a small unheated area between the humps. Let us also compare the heat fluxes from the surface (the functions $w(\xi, t)$), see (36). It can be seen in Fig. 10 that the temperature gradient is naturally smaller with a smaller region of maximal heating (see the red curve) and the extremum points are also shifted: for the function $T_{\Gamma,1}(\xi)$, they are located in the region of the front edges of the humps (see the black curve), and for the function $T_{\Gamma,2}(\xi)$, they are located near the tops of the humps. Note that, for a wider heating region given by the piecewise constant function $T_{\Gamma,3}$, the plot is completely different (see the blue curve).

Now we consider the step-like shape of the irregularity:

$$h_3(\xi) = 2.5 * \big(2 + \tanh\big((x+2)3\big)\tanh\big((2-x)3\big) + \tanh\big((x-6.5+2)3\big)\tanh\big((2.0-(x-6.5))3\big)\big), \tag{41}$$

see Fig. 11.

The simulation results for this shape of the irregularity and the heating function $T_{\Gamma,1}(\xi)$ (see (38)) are shown in Fig. 12 for the case when the heating is turned on after the steady flow has been established (see Fig. 12 (a)). It can be seen that the presence of the vortex that fills the entire space between the steps prevents the heated flow from penetrating into this region, see Fig. 12 (c)–(e). Note that the vortices are reflected in the streamlines. Namely, we observe that they have small extrema in the region above the left boundaries of both vortices and the right boundary of the left vortex (see Fig. 12), and these extrema are also reflected in temperature isolines, see Fig. 12 (b)–(e), and in the surface heat flux function $w(\xi, t)$, see Fig. 12 (f). The comparison with the case of irregularity in the form of two humps of the same height $h_2(\xi)$ (see (39)) in Fig. 7 shows the faster propagation of the heated fluid along the flow in the case of the irregularity shape $h_3(\xi)$, the magnitude of the heat flux from the surface is approximately the same in these cases, but the plots are different, see Fig. 12 (f).

Finally, we study the heat transfer in the flow around holes with heated bottom. As a function describing the irregularity, we take the function $h_4(\xi) = -h_3(\xi)$ (see (41)), and as a function describing the heating of the streamlined surface, the function $T_{\Gamma,1}(\xi)$, see (38). We will turn on the heating after the flow has reached the steady state (see Fig. 13 (a)). The simulation results for the Prandtl number $\mathrm{Pr} = 0.1$ are shown in Fig. 13. It can be seen that, as in the previous case (see Fig. 12), there are some small extrema on the streamlines as a result of the presence of stationary vortices in the holes, which are also reflected in the temperature isolines. We also note that the temperature trace from the second hole at time $t = 20$ is larger (see 13 (c)), because the heated flow from the first hole comes into it by this time due to its drift along the flow.

5 Conclusions

In this paper, we study heat transfer in the framework of the double-deck boundary layer structure for the problem of a viscous incompressible fluid flow along a plate with small localized heated irregularities on its surface. The asymptotic solution of the considered problem is constructed (see Theorem 1) for large Reynolds numbers. The results of numerical simulation (see Section 4) are presented depending on various parameters of the problem. In particular, the heat removal from the streamlined surface has been studied in view of the fact that one of the possible real applications of the constructed mathematical model is the cooling of any small-sized devices.

Funding The work was supported by the Russian Science Foundation under grant No. 19-71-10003.

Declarations

Conflict of interest The authors declare that they have no conflict of interest.

References

1. Stewartson, K., Williams, P.G.: Self-induced separation. Proceedings of the Royal Society A 312, 181–206 (1969)
2. Neiland, V.Y.: Theory of laminar boundary layer separation in supersonic flow. Fluid Dynamics 4, 33–35 (1969)
3. Smith, F.T.: Laminar flow over a small hump on a flat plate. Journal of Fluid Mechanics 57, 803–824 (1973)
4. Mauss, J.: Asymptotic modelling for separating boundary layers. Lecture Notes in Physics 442, 239–254 (1995)
5. Danilov, V.G., Makarova, M.V.: Asymptotic and numerical analysis of the flow around a plate with small periodic irregularities. Russian Journal of Mathematical Physics 2, 49–56 (1994)

6. Mengaldo, G., Kravtsova, M., Ruban, A.,, Sherwin, S.: Triple-deck and direct numerical simulation analyses of high-speed subsonic flows past a roughness element. Journal of Fluid Mechanics 774, 311–323 (2015)
7. Lipatov, I.I.: Disturbed boundary layer flow with local time-dependent surface heating. Fluid Dynamics 41(5), 725–735 (2006)
8. Koroteyev, M.V., Lipatov, I.I.: Steady subsonic boundary layer in domains of local surface heating. Journal of Applied Mathematics and Mechanics 77(5), 486–493 (2013)
9. Koroteev, M.V., Lipatov, I.I.: Local temperature perturbations of the boundary layer in the regime of free viscous-inviscid interaction. Journal of Fluid Mechanics 707, 595–605 (2012)
10. Koroteev, M.V., Lipatov, I.I.: Supersonic boundary layer in regions with small temperature perturbations on the wall. SIAM Journal on Applied Mathematics 70(4), 1139–1156 (2009)
11. Aljohani, A.F., Gajjar, J.S.B.: Subsonic flow past localised heating elements in boundary layers. Journal of Fluid Mechanics 821, 2 (2017)
12. Aljohani, A.F., Gajjar, J.S.B.: Transonic flow over localised heating elements in boundary layers. Journal of Fluid Mechanics 844, 746–765 (2018)
13. Danilov, V.G., Gaydukov, R.K.: Double-deck structure of the boundary layer in problems of flow around localized perturbations on a plate. Mathematical Notes 98, 561–571 (2015)
14. Gaydukov, R.K.: Double-deck structure in the problem of a compressible flow along a plate with small localized irregularities on the surface. European Journal of Mechanics – B/Fluids 71, 59–65 (2018)
15. Gaydukov, R.K.: Double-deck structure in the fluid flow problem over plate with small irregularities of time-dependent shape. European Journal of Mechanics-B/Fluids 89, 401–410 (2021)
16. Danilov, V.G., Gaydukov, R.K.: Vortices in the prandtl boundary layer induced by irregularities on a plate. Russian Journal of Mathematical Physics 22, 161–173 (2015)
17. Gaydukov, R.K., Danilov, V.G.: Equations for velocity oscillations in problems of a fluid flow along a plate with small periodic irregularities on the surface for large Reynolds numbers. In: Proceedings of the International Conference DAYS on DIFFRACTION 2018, pp. 118–123 (2018)
18. Gaydukov, R.K., Danilov, V.G.: Multideck structures of boundary layers in compressible flows. In: Proceedings of the International Conference DAYS on DIFFRACTION 2019, pp. 51–56 (2019)
19. Vishik, M.I., Lyusternik, L.A.: Regular degeneration and boundary layer for linear differential equations with small parameter. Uspekhi Mat. Nauk 12, 3–122 (1957)
20. Schlichting, H., Gersten, K.: Boundary-layer Theory. Springer, Berlin (2016)
21. Desale, S., Pradhan, V.H.: Numerical solution of boundary layer flow equation with viscous dissipation effect along a flat plate with variable temperature. Procedia Engineering 127, 846–853 (2015)
22. Roache, P.J.: Fundamentals of Computational Fluid Dynamics. Hermosa Publishers, Albuquerque (1976)
23. Yapalparvi, R.: Double-deck structure revisited. European Journal of Mechanics - B/Fluids 31, 53–70 (2012)
24. Gaydukov, R.K.: A numerical algorithm for solving the prandtl equations with induced pressure in the periodic case. Numerical Analysis and Applications 15, 79–89 (2022)